Application of a Channelized Energy Detector for Digital Wideband ESM Receivers

Aline de Oliveira and Jorge Pires and Rodrigo Moreira

***Abstract*— It is not an easy job to select and adjust a general-purpose detector for digital wideband Electronic Support Measures (ESM) receivers. Optimal detectors and parameters' adjustment depend on many variables, e.g., the receiver characteristics, application and system's constraints. In this paper, we study the performance of a FFT-based channelized energy-based detector (CED) for ESM receivers, in which time integration is based on logic-OR and binary integration. We show that, for the studied Electronic Warfare scenario, the CED outperforms other detectors: total energy, GLRT and ambiguity function-based detectors. This investigation points the CED as an interesting option for ESM receivers.**

***Keywords*— Electronic Support Measures (ESM), Electronic Warfare (EW), Digital Receiver, energy detection, channelized energy-based detection, FFT-based channelized receiver.**

I. Introduction

Within the field of Electronic Warfare (EW), the Electronic Support Measures (ESM) division holds the task of passively intercepting, identifying, and locating sources of hostile radiations [1]. ESM receivers passively exploit the electromagnetic emissions within a very large bandwidth, without any *a priori* knowledge, to provide information for tactical picture compilation in the battle theater.

This study assumes a Wideband Digital Receiver ESM architecture which employs a tunable Superheterodyne receiver, with a large instantaneous bandwidth, followed by a high-speed analog-to-digital converter (ADC), which is able to sample the in-phase and quadrature (I and Q) channels. The digitized samples enter the signal processing block, where the detection algorithms take place. These conditions enable the collection of many samples of the same signal, allowing the detection to take place not only in time, but also in frequency domain, which may improve detection performance [2].

The optimal detector for pulses with unknown phase, carrier frequency, amplitude and time of arrival is the Generalized Likelihood Ratio Test (GLRT) [3], which ends up testing the spectrogram values. In [4], the authors have added a binary integration detection strategy to the spectrogram values along the time axis which improved the robustness against spurious signals, but is not adequate for the detection of Linear Frequency Modulated (LFM) signals. In [5], the authors proposed a detector based on the Ambiguity Function, which is linked to the Cross Wigner-Ville distribution [6] in a causal form [7], therefore, suitable for detecting LFM signals.

In this paper, we propose a channelized energy-based detector, with a detection strategy based in logic-OR and binary integration (CED), where channelization is achieved by a Fast Fourier Transform (FFT) pre-processor and compare it with other detectors: total energy (TED), GLRT, and the ambiguity-based detector of [5]. Computer simulations shows that with an adequate choice of parameters, the CED has superior detection performance, even for LFM signals.

This paper is organized as follows: the system model is described in Section II; the CED is explained in Section III, a review of the other detection methods is in Section IV. Computer simulations are presented in Section V and, finally, conclusions are given in section VI.

Aline de Oliveira, Jorge Pires, Rodrigo Moreira, Instituto de Pesquisas da Marinha (IPqM), Rio de Janeiro, e-mail:{aline.oliveira; jorge.costa; silva.moreira}@marinha.mil.br

II. System Model

Consider a radar signal, $s(t)$, with a carrier frequency, f_c,

$$s(t) = Ag(t)\cos(2\pi f_c t + \phi(t) + \psi), \tag{1}$$

where A is the signal amplitude in Volts, $g(t)$ is a gate function with width τ (starting at the origin) and unitary amplitude, $\phi(t)$ is the intrapulse modulation function and ψ is the initial phase. The received signal within a data processing frame (DPF) of duration T_{DPF} is $r(t)$,

$$r(t) = s(t-T) + n(t),\ 0 \le t \le T_{\text{DPF}}, \tag{2}$$

where $n(t)$ is an AWGN process with variance σ_n^2 and T is the Time of Arrival (TOA). The received signal, $r(t)$, is downconverted to an intermediary frequency f_I and digitized with a Nyquist-compliant sampling frequency, f_s, where its in-phase (I) and quadrature (Q) samples form the complex received pulse sequence, $r[n]$,

$$r[n] = r(nt_s), \tag{3}$$

where t_s is the sampling period, $t_s = 1/f_s$.

A. Binary Detection Problem

The binary signal detection problem is a hypothesis testing problem, whose goal is to decide between the null hypothesis, $\mathcal{H}_0$ (noise only case) and the alternative hypothesis, $\mathcal{H}_1$ (presence of the signal of interest). Using a digital receiver, the decision can be made upon a sequence of N complex samples from (3) stacked as a column vector, $\mathbf{r} \in \mathbb{C}^{N\times 1}$:

$$\begin{aligned} \mathcal{H}_0 &: \mathbf{r} = \mathbf{n}, \\ \mathcal{H}_1 &: \mathbf{r} = \mathbf{s} + \mathbf{n}. \end{aligned}$$

Detection is based on some function $T(\cdot)$ of the received vector, the decision variable, which is compared to a threshold, η. If $T(\mathbf{r})$ exceeds the threshold, then hypothesis $\mathcal{H}_1$ is chosen. Different functions $T(\cdot)$ imply in different detectors.

III. Channelized Energy Detector

The object of this study is the FFT-based channelized energy detector (CED) which can work with time integration. The detection strategy for the time integration employs logical-OR and binary integration. Loosely speaking, the CED is a detection scheme employed in receivers with filter bank arrays, in which the output of several parallel narrowband reception filters are combined to result in a final decision. An integration interval, T_R, which is a fraction of the total observation interval, may also be applied, which allows many different decision strategies to combine the output of the individual receivers [8]. The channelized receiver can be similarly implemented with Fast Fourier Transform (FFT) front-end preprocessor, by summing some adjacent time and/or frequency spectrogram bins [9], [10].

Fig. 1 illustrates the idea of a channelized energy detector implemented with FFTs, which can be viewed as a partition of the spectrogram. Each big rectangle corresponds to a time-frequency cell of the channelized receiver. The decision variable, $V_{i,j}$, of each individual time-frequency cell is the sum of the spectrogram values inside the partitioned region $S_{i,j}$, correspondent to the i-th channel and j-th interval,

$$V_{i,j} = \frac{1}{\sigma_n^2} \sum_{(m,l)\in S_{i,j}} |I_{n_l}(f_m)|^2, \tag{4}$$

where $I_{n_l}(f_m)$, are the entries of the spectrogram matrix,

$$I_{n_l}(f_m) = \frac{1}{\sqrt{N_{\text{FFT}}}} \sum_{k=0}^{N_{\text{FFT}}-1} r((l-1)N_{\text{FFT}}+k)\exp\left\{\frac{-\text{j}2\pi km}{N_{\text{FFT}}}\right\}, \tag{5}$$

N_{FFT} is the number of FFT points, f_m is the m-th FFT frequency bin $f_m = mf_s/N_{\text{FFT}}$ and n_l corresponds to the l-th time interval, $[(l-1)N_{\text{FFT}}t_s,\ lN_{\text{FFT}}t_s]$.

The real and imaginary parts of $I_{n_l}(f_m)$, are jointly Gaussian independent variables with variance σ_n^2; under hypothesis $\mathcal{H}_0$, the mean of both real and imaginary parts is zero. Under hypothesis $\mathcal{H}_1$, the mean of the real and imaginary parts of $I_{n_l}(f_m)$ depends on the type of signal present during the observation interval. The best case scenario, in terms of energy concentration in the spectrogram cell, is the presence of an unmodulated signal with carrier frequency $f_c = f_m$ occupying the complete n_l interval. In this case, the expected value of the magnitude squared of $I_{n_l}(f_m)$ is $\text{E}\left[|I_{n_l}(f_m)|^2\right] = N_{\text{FFT}}A^2$, where A is the pulse amplitude.

Assuming the distributions of [11], the decision variable $V_{i,j}$, under the noise-only case, $p(v_{i,j}|\mathcal{H}_0)$, follows the chi-squared distribution, $\chi^2_\nu(v)$, where $\nu = 2M$ is the number of the chi-squared degrees of freedom and M is the number of summands in (4). Dropping the indexes, since under the noise-only case, $V_{i,j}$ are independent and identically distributed, $p(v|\mathcal{H}_0)$, is given by $\chi^2_\nu(v)$,

$$\chi^2_\nu(v) = \frac{v^{\frac{\nu-2}{4}}e^{-\frac{v}{2}}}{(2)^{\frac{\nu}{2}}\Gamma(\nu/2)}, \tag{6}$$

where $\Gamma(\cdot)$ is the gamma function. The *probability of false alarm of a time-frequency cell*, Q, is the probability of the decision variable, $V_{i,j}$, being above a threshold η for the noise-only case, that is

$$Q = F_{\chi^2}(\eta; 2M), \tag{7}$$

where $F_{\chi^2}(x;\nu)$ is the chi-squared cumulative distribution function.

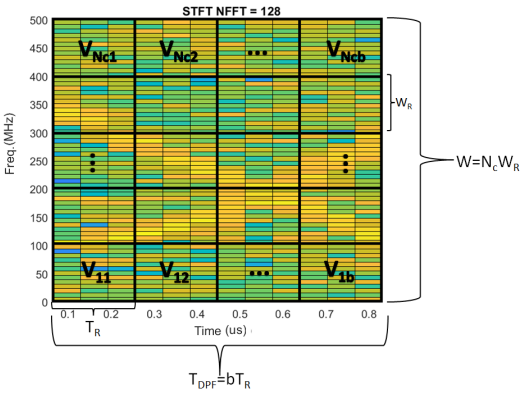

Fig. 1: Representation of a channelized receiver using a STFT.

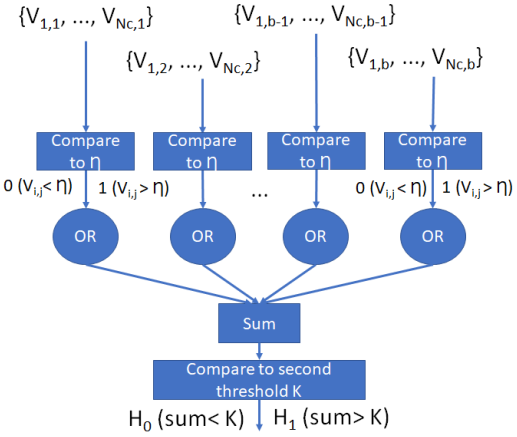

Fig. 2: Diagram of the detection strategy: binary integration over the logic-OR column's outputs.

Although the optimum detection strategy for combining the output of the receiver's channels and integration intervals is the Average Likelihood Ratio (ALR) detector [12], [13], or equivalently, for this case, the Woodring-Edell (WE) detector [14], we adopt a suboptimal method based on logical-OR and binary integration which is more easily analysed, implemented and is not SNR dependent as the optimal detector. The detection strategy adopted in this study is described in [15] under the name OR/BMWD (logical-OR and Binary Moving Window Detector) which performs similarly as the ALR detector [16].

The performance comparison of the methods in this paper is made in a block detection scheme, therefore, the detection strategy of [15] is explained here for a fixed time window of duration T_{DPF}. In Fig. 1 there are N_C frequency channels, and b integrations intervals, $b = T_{\text{DPF}}/T_R$, thus, the total number of time-frequency cells is $N_{\text{total}} = N_C b$. Each cell is tested with the threshold η, which implies in a certain cell probability of false alarm, Q, (whose computations are explained later on).

Fig. 2 illustrates the detection strategy: a) a hard decision is made for each $V_{i,j}$; b) a logical-OR is implemented column-wise; c) if at least K columns are "positive" for detection, then the decision over the block in test is for hypothesis $\mathcal{H}_1$, presence of pulse.

The *probability of false alarm of a column*, p_0, is the probability of at least one of the N_c cells of the column being above the threshold in a noise-only scenario,

$$p_0 = 1 - (1 - Q)^{N_C}. \tag{8}$$

The *final probability of false alarm*, P_f can be computed as

$$P_f = \sum_{k=K}^{N} \binom{N}{k} p_0^k (1 - p_0)^{N-k}. \tag{9}$$

Given the system probability of false alarm, P_f, one can compute p_0 iteratively [17]. After computing p_0, one can compute the cell probability of false alarm, Q using (8) and the threshold, η, as the inverse of (7).

IV. Review of the other Detectors

In this section, we present the detectors implemented in this paper for comparison purpose.

A. Ambiguity-based Detector

This subsection briefly explains the detector proposed in [5]. This detector is inspired by the Ambiguity Function, $AF(n_T, f)$, defined in [5] as

$$AF(n_T, f) = \sum_{k=0}^{N_I - 1} x[k + n_T] x^*[k] e^{-i2\pi f \frac{k}{fs}}, \tag{10}$$

where n_T is the delay, f is the frequency, $N_I = N - n_T$ and N is the length of the complex waveform sequence $x[k]$. The idea of this detector is illustrated in Figs. 3 and 4. Fig. 3 depicts the magnitude of the Ambiguity Function (AF) of an unmodulated pulse (left) and a chirp (right) with a slope α of 67 MHz/μs, both with 1 μs duration. As expected, the AF of the unmodulated pulse looks like a straight line and the chirp AF is tilted with an inclination corresponding to the chirp slope.

If one cuts the AF at a certain delay, say τ_c, then the plot of this view depicts the magnitude as function of the frequency, f. Fig. 4 depicts the AFs' cut for a 0.1 μs delay, τ_c = 0.1 μs. We can observe a peak at frequency zero for the unmodulated pulse (left) and a peak at frequency, f_p, far from zero, for the chirp (right), where f_p is proportional to the chirp slope, α, $f_p = \alpha\tau_c$. Note the same magnitude for both peaks, that is because this detector does not "spread" the chirp energy, as it happens with FFT-based detectors when it comes down to detecting chirps.

The probability density function of the decision variable given by $D = |AF(n_T, f)|/N_I$, $AF(n_T, f)$ defined in (10) under the noise-only case, $p(d|\mathcal{H}_0)$, is given by [18]

$$p(d|\mathcal{H}_0) = \frac{4N_I^{N_I+1} d^{N_I}}{\Gamma(N_I)\sigma_n^{2N_I+2}} I_0(0)\, K_{N_I-1}\left(\frac{2N_I d}{\sigma_n^2}\right), \tag{11}$$

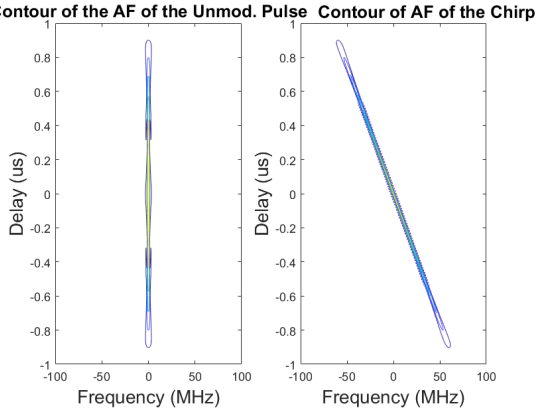

Fig. 3: Example of the Contour of the AF for a pulse (left) and a chirp (right) without noise.

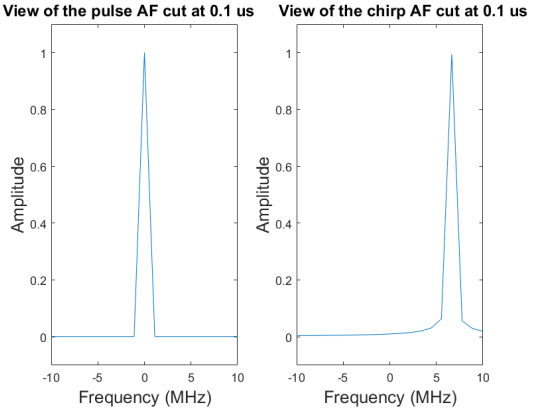

Fig. 4: View of a cut at 0.1 μs of the AFs in 3.

where $I_0(\cdot)$ and $K_\nu(\cdot)$ are modified Bessel functions. The *probability of false alarm*, Q, *for a given frequency*, $f = f_m$, is

$$Q = \Pr\{d > \eta | \mathcal{H}_0\} = \int_{d=\eta}^{\infty} p(d|\mathcal{H}_0) \mathrm{d}d. \tag{12}$$

A false alarm occurs if the decision variable $|AF(n_T, f_m)|/N_I$ of any one of the computed frequencies, f_m, $m = 1, \ldots, N_F$, for a fixed delay, n_T, is above the threshold. The *total probability of false alarm*, P_f, is given by

$$P_f = 1 - (1 - Q)^{N_F}. \tag{13}$$

Given the system probability of false alarm, P_f, one can compute Q from (13) and η can be found by numerical integration of (11), there are computational difficulties for large values of N_I though. Thus, we established the threshold through Monte Carlo simulations in this paper.

B. Total Energy Detector

The decision variable of the total energy detector (TED) in this paper is

$$V = \frac{1}{\sigma_n^2} \sum_{k=0}^{N-1} |r[k]|^2, \tag{14}$$

where $r[k]$ is the k-th component of the digitized received vector $\mathbf{r} \in \mathbb{C}^{N \times 1}$. Assuming the distributions of [11],

the decision variable V under the noise-only case, $p(v|\mathcal{H}_0)$ follows the chi-squared distribution, $\chi^2_\nu(v)$, described in (6), where $\nu = 2N$. Given a total system probability of false alarm, P_f, the threshold of the total energy detector, η, is given by the inverse of the chi-squared cumulative distribution function, $F_{\chi^2}(x;\nu)$, as

$$\eta = F^{-1}_{\chi^2}(1 - P_f; 2N). \tag{15}$$

C. GLRT Detector

The Generalized Likelihood Ratio Test (GLRT) for detecting sinusoidal pulses with unknown parameters corrupted by AWG noise resumes to the comparison of the short-time Fourier Transform (STFT) or spectrogram [3] to a threshold, η. The GLRT detector decides for hypothesis H_1 (presence of pulse) if

$$\max_{n_l, f_m} |I_{n_l}(f_m)| > \eta, \tag{16}$$

where $I_{n_l}(f_m)$ are the entries of the spectrogram matrix, described in (5), which are Rayleigh distributed in the noise-only case. If one searches among N_{total} entries, (n_l, f_m) pairs, than the threshold, η, which results in a total probability of false alarm, P_f, is directly given by

$$\eta = \sqrt{-\sigma_n^2 \ln\left(1 - \sqrt[N_{\text{total}}]{1 - P_f}\right)}. \tag{17}$$

where $\ln(\cdot)$ is the natural logarithm.

D. Genie-aided Matched Filter Detector

The genie detector is a matched filter with perfect knowledge of the received signal (obtained from a genie). The decision variable, V, is

$$V = \frac{|y[N]|}{\sqrt{N}}, \tag{18}$$

where $y[N]$ is $y[k]$ for $k = N$ and $y[k] = r[k] * f_M[k]$, where $f_M[k]$ is the filter matched to the received signal, $s[k]$, $f_M[k] = s^*[-k]$, and N is the length of the signal sequence $s[k]$. In the noise-only case, the decision variable, V, is Rayleigh distributed, thus for a total probability of false alarm, P_f, the threshold η is directly given by

$$\eta = \sqrt{-2\sigma_n^2 \ln(P_f)}. \tag{19}$$

where $\ln(\cdot)$ is the natural logarithm.

V. Simulation

We compare the performance of four detectors: the Ambiguity-based detector (Amb. Met.), explained in Subsection IV-A, the TED, explained in IV-B, the GLRT, explained in IV-C, and, finally, the CED, which is the object of this study and is detailed explained in Section III. The Genie MF, explained in IV-D, is plotted as an **upper bound**.

The proposed simulation considers a data processing frame (DPF) of 1 μs, T_{DPF} = 1 μs and the SNR is defined as $A^2/2\sigma_n^2$. In order to verify the performance of the detectors, we simulate with MATLAB different illustrative scenarios in the context of EW: chirps with different slopes, unmodulated and Barker-13 pulses.

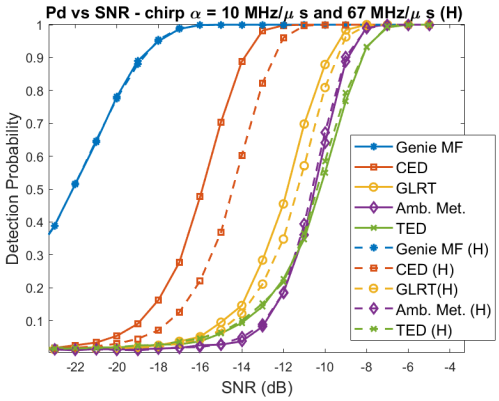

Fig. 5: Pd vs. SNR curves for chirp with a slope of α = 10 MHz/μs and a larger slope of α = 67 MHz/μs, described in the legend with (H).

The parameters of the CED were empirically optimized for N_{FFT}=64, T_{DPF} = 1 μs and $f_s = 1$ GHz. The CED architecture which results in best performance is, actually, without the time axis division, $T_R = T_{\text{DPF}}$. This is an interesting fact and further investigations can be done in this sense, maybe for longer DPFs the results are different. The number of frequency bins added together in order to form the time-frequency cell is three, resulting in a frequency bandwidth of $W_R = 3f_s/N_{\text{FFT}}$.

For the Ambiguity-based Detector, we limited the search scope to the frequencies associated to a slope range of $|\alpha| \leq$ 100 MHz/μs and defined a delay of 0.1 μs. The number of summands for the TED is equal to N_I in the Ambiguity-based Detector. The number of FFT points N_{FFT} for the GLRT and for the CED are the same and equal to 64.

The threshold of all detectors are established for a false alarm rate of R_f = 0.01μs^{-1}, which implies in a false alarm probability of $P_f = 0.01$ per DPF. The false alarm is large to facilitate simulations.

Fig. 5 depicts the curves of probability of detection (Pd) vs. SNR for chirps with slopes of 10 and 67 MHz/μs respectively. One can see that the CED performs much better than the other detectors. It is interesting to note that the CED performs better for slope 10 MHz/μs than for 67 MHz/μs. That is because, for larger slopes, the chirp energy is more spread in frequency, as illustrated in Figs. 6 and 7, which depict the 0 dB SNR spectrogram of the chirps with slopes 10 and 67 MHz/μs respectively. Fig. 8 shows the Pd vs. SNR for different slopes (an unmodulated pulse corresponds to α = 0 MHz/μs), one can note the gain in detection for reducing the slope.

Fig. 9 depict the Pd. vs. SNR for an unmodulated pulse occupying the entire DPF. The CED still has superior performance than the other detectors. As expected, the Amb. Met. performs identically for the unmodulated pulse of Fig. 9 and for the chirps with different slopes of Fig. 5, since, as illustrated in Fig. 4, the energy of both types of signals is concentrated, just in different frequencies.

Fig. 10 depicts the Pd. vs. SNR for a complete Barker 13 code within the DPF interval. The CED outperforms the other

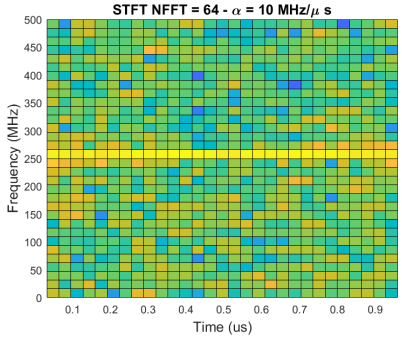

Fig. 6: α = 10 MHz/μs. SNR = 0 dB.

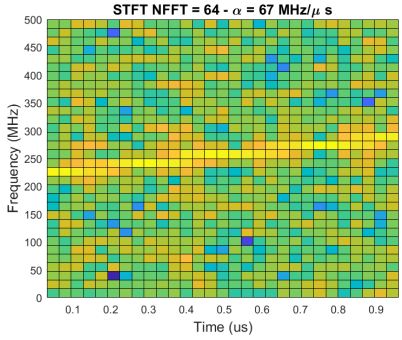

Fig. 7: α = 67 MHz/μs. SNR = 0 dB.

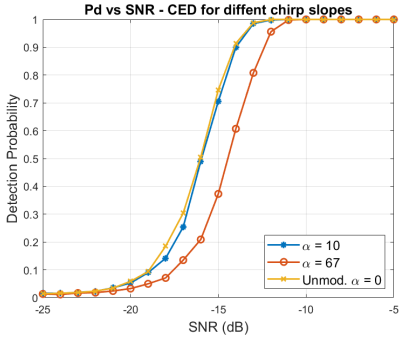

Fig. 8: CED Pd vs. SNR for different α.

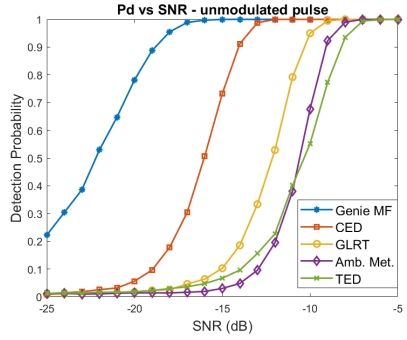

Fig. 9: Pd vs. SNR for unmod. pulse.

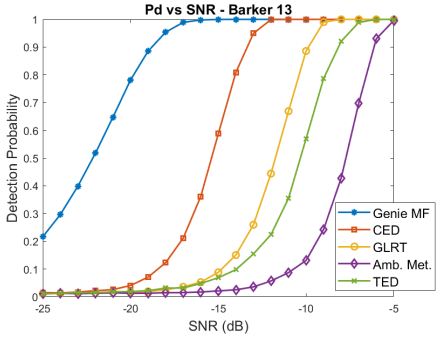

Fig. 10: Pd vs. SNR for Barker 13.

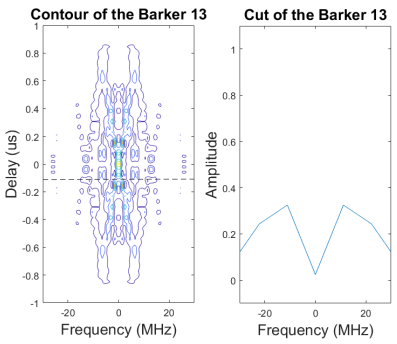

Fig. 11: Barker 13 AF and cut at 0.1 μs.

detectors and the Amb. Met. performs poorly. That is because the cut at the chosen delay is not adequate for the Ambiguity Function of the barker 13 as shown in Fig. 11.

VI. Conclusions

This paper studies a FFT-based Channelized Energy Detector with detection strategy based on logic-OR and binary integration (CED) for EW scenarios which is computationally simple and FPGA friendly. Simulations show that with an adequate choice of parameters, it considerably outperforms other detectors: a total energy detector, a GLRT detector and an Ambiguity-based detector [5]. This initial investigation points the CED as an interesting choice for a general purpose detector for ESM receivers in the context of EW. An EW-oriented methodology for the parameters' selection is left for future work, figures of merit in [15] could be a start point.

References

[1] D. Curtis Scheleher, *Introduction to Electronic Warfare*, Artech House, 1986.

[2] James Tsui and Chi-Hao Cheng, *Digital Techniques for Wideband Receivers*, Scitech Publishing an imprint of the IET, 3 edition, 2016.

[3] Steven M. Kay, *Fundamentals of Statistical Signal Processing: Detection theory*, vol. II of *Prentice-Hall Sig. Proc. Series*, Prentice-Hall, 1998.

[4] A. de Oliveira and J. Pires, "A novel detection method of unmodulated radar pulses in scenarios with interference for digital wideband esm receivers," in *2019 16th European Radar Conference (EuRAD)*, 2019, pp. 61–64.

[5] A. Foucault, C. Cornu, A. Khenchaf, and F. Comblet, "Detection of linear frequency modulation, phase-coded and multicarrier radar waveforms in electronic warfare context," in *2020 Sensor Signal Processing for Defence Conference (SSPD)*, 2020, pp. 1–5.

[6] S. A. Elgamel, C. Clemente, and J. J. Soraghan, "A time-frequency formulation of optimum detection 1988," in *Sensor Signal Proc. for Defence (SSPD 2010)*, Sep. 2010, pp. 1–5.

[7] Philip E. Pace, *Detecting and Classifying Low Probability of Intercept Radar*, Artech House, second edition, 2009.

[8] Janne Lehtomaki, *Analysis of energy based signal detection*, Ph.D. thesis, University of Oulu, 2005.

[9] D. Cabric, S.M. Mishra, and R.W. Brodersen, "Implementation issues in spectrum sensing for cognitive radios," in *Conference Record of the Thirty-Eighth Asilomar Conference on Signals, Systems and Computers, 2004.*, 2004, vol. 1, pp. 772–776 Vol.1.

[10] B. Levitt, M. Simon, A. Polydoros, and C. Unjeng, "Partial-band detection of frequency-hopped signals," in *Proceedings of GLOBECOM '93. IEEE Global Telecommunications Conference*, 1993, pp. 70–76 vol.4.

[11] H. Urkowitz, "Energy detection of unknown deterministic signals," *Proceedings of the IEEE*, vol. 55, no. 4, pp. 523–531, 1967.

[12] VanTrees, *VanTrees*, McGraw-Hill, New York, 4th ed. edition, 2001.

[13] R.A. Dillard and G.M. Dillard, "Likelihood-ratio detection of frequency-hopped signals," *IEEE Transactions on Aerospace and Electronic Systems*, vol. 32, no. 2, pp. 543–553, 1996.

[14] B.K. Levitt, Unjeng Cheng, A. Polydoros, and M.K. Simon, "Optimum detection of slow frequency-hopped signals," *IEEE Transactions on Communications*, vol. 42, no. 234, pp. 1990–2000, 1994.

[15] R.A. Dillard, "Detectability of spread-spectrum signals," *IEEE Transactions on Aerospace and Electronic Systems*, vol. AES-15, no. 4, pp. 526–537, 1979.

[16] N.C. Beaulieu, P.J. McLane, and W.L. Hopkins, "Interception of frequency hopped spread spectrum signals," in *IEEE International Conference on Communications, Including Supercomm Technical Sessions*, 1990, pp. 641–648 vol.2.

[17] L.E. Miller, J.S. Lee, and D.J. Torrieri, "Frequency-hopping signal detection using partial band coverage," *IEEE Transactions on Aerospace and Electronic Systems*, vol. 29, no. 2, pp. 540–553, 1993.

[18] J-S. Lee, K.W. Hoppel, S.A Mango, and A.R. Miller, "Intensity and phase statistics of multilook polarimetric and interferometric sar imagery," *IEEE Transactions on Geoscience and Remote Sensing*, vol. 32, no. 5, pp. 1017–1028, September 1994.